Phase transitions and slow spin dynamics of slightly inverted A-site spinel $CoAl_{2-x}Ga_xO_4$

T. Naka[1, *], J. Valenta,[1] T. Nakane,[2] S. Ishii,[3] M. Nakayama,[1] H. Mamiya,[4] K. Takehana,[5] N. Tsujii,[1] Y. Imanaka,[5] Y. Matsushita,[6] H. Abe,[7] T. Uchikoshi,[2] and H. Yusa[1]

[1]*Research Center for Materials Nanoarchitectonics, National Institute for Materials Science, 1-2-1, Sengen, Tsukuba, Ibaraki 305-0047, Japan*
[2]*Research Center for Electronic and Optical Materials, National Institute for Materials Science, 1-2-1, Sengen, Tsukuba, Ibaraki 305-0047, Japan*
[3]*Department of Physics, Tokyo Denki University, Hatoyama, Saitama 350-0394, Japan*
[4]*Research Center for Magnetic and Spintronic Materials, National Institute for Materials Science, 1-2-1, Sengen, Tsukuba, Ibaraki 305-0047, Japan*
[5]*Center for Basic Research on Materials, National Institute for Materials Science, 1-2-1, Sengen, Tsukuba, Ibaraki 305-0047, Japan*
[6]*Research Network and Facility Services Divisions, National Institute for Materials Science, 1-2-1, Sengen, Tsukuba, Ibaraki 305-0047, Japan*
[7]*Joint and Welding Research Institution, Osaka University, 11-1 Mihogaoka, Ibaraki, Osaka 567-0047, Japan*

We report the properties of an A-site spinel magnet, $CoAl_{2-x}Ga_xO_4$, and analyze its anomalous, low-temperature magnetic behavior, which is derived from inherent, magnetically frustrated interactions. Rietveld analysis of the x-ray diffraction profile for $CoAl_{2-x}Ga_xO_4$ revealed that the metallic ions were randomly distributed in the tetrahedral (A-) and octahedral (B-) sites in the cubic spinel structure. The inversion parameter η could be controlled by varying the gallium (Ga) composition in the range $0.055 \leq \eta \leq 0.664$. The composition-induced Néel-to-spin-glass (NSG) transition occurred between $0.05 \leq \eta \leq 0.08$ and was verified by measurements of DC-AC susceptibilities χ and thermoremanent magnetization (TRM) below the Néel transition temperature T_N. The relaxation rate and derivative with respect to temperature of TRM increased at both T_N and the spin glass (SG) transition temperature T_{SG}. The TRM decayed rapidly above and below these transitions. TRM was highly sensitive to macroscopic magnetic transitions that occurred in both the Néel and SG phases of $CoAl_{2-x}Ga_xO_4$. In the vicinity of the NSG boundary, there was a maximum of the TRM relaxation rate at $T_{max} < T_N$. With increasing inversion $\eta(x)$, the anomaly at T_{max} merged with that of the Néel transition at a tricritical point $(\eta_{tc}, T_{tc}) = (0.08, 4.0\ K)$, where the paramagnetic, Néel, and SG states met. We successfully extracted the relaxation time τ and other characteristic

parameters from the TRM isothermal temporal evolution based on the Weron function derived for a purely stochastic process. To distinguish the magnetic states, we compared our results with previously studied inversion-free A-site spinel, $CoRh_2O_4$, and $CoGa_2O_4$ cluster glass. We generated an inversion-temperature phase diagram based on the comprehensive measurements of DC and AC susceptibilities, TRM, and specific heat in the range $0.055 \leq \eta \leq 0.664$ for $CoAl_{2-x}Ga_xO_4$. Based on this phase diagram, we speculate that a NSG quantum critical phase transition occurred at $\eta = 0.050(6)$. Our findings are consistent with suppression of the long-range order antiferromagnetic state in $CoAl_2O_4$ revealed through neutron diffraction studies, even at $T << T_N$.

*naka.takashi@nims.go.jp

I. INTRODUCTION

Nanoscale objects (nano-objects) embedded in matrix materials induce remarkable thermomagnetic phenomena, such as exchange bias and thermoremanent magnetization (TRM) [1]. Magnetization of nano-objects in such materials make them behave as complex systems that depend on the type of experimental pretreatment (i.e., magnetic, thermal, and temporal histories) [2]. These magnetized nano-objects (magnetic clusters) create disorders in the matrix material that often qualitatively alter its ground state. A recent study has revealed that such magnetic clusters due to disorders (anti-site defects) in the magnetically frustrated A-site spinel antiferromagnet can act as highly sensitive probes for magnetic phase transitions [3]. Such disorders and magnetic interactions in A-site spinel magnets induce specific relaxation phenomena in both antiferromagnetic (AF) and spin glass (SG) states. From the temperature and time dependencies of TRM, important information can be extracted about magnetic phase transitions and spin dynamics in A-site spinel magnets with formula unit compositions of CoM_2O_4, where M = Al, Rh, and Ga correspond to strongly frustrated antiferromagnets, weakly frustrated antiferromagnets, and cluster glasses (CGs), respectively [3]. The derivative of the TRM intensity, M_{TR}, with respect to temperature $(1/M_{TR})(dM_{TR}/dT)$ and the relaxation rate $\Delta M_{TR}(t)/M_{TR}(0)$ are highly sensitive to magnetic transitions, irrespective of the magnetic state and the degree of magnetic frustration.

In this paper, we demonstrate the application of TRM measurements to study magnetic disorder effects in gallium-substituted cobalt aluminate ($CoAl_{2-x}Ga_xO_4$), and we compare them with those of the disorder-free, A-site spinel antiferromagnet cobalt rhodate ($CoRh_2O_4$) [4] and a cobalt gallate CG ($CoGa_2O_4$) [5]. In the spinel oxide $CoAl_2O_4$, divalent Co^{2+} and trivalent Al^{3+} ions occupy the tetrahedral (A-) and octahedral (B-) sites, respectively. The A-site forms a magnetically bipartite diamond lattice consisting of two interpenetrated face-centered cubic (FCC) lattices that are shifted along the [111] direction. A nearest-neighbor interaction J_1 is hence realized between Co^{2+}-spins located at the A-sites of different FCC lattices. Simultaneously, a next-nearest-neighbor interaction J_2 is established between Co^{2+} spins located at the A-sites within the same FCC lattice. Note that, therefore, a diamond lattice is bipartite and the A-site antiferromagnet exhibits a Néel-type antiferromagnetic spin structure when $J_1 >> J_2$. Contrary, a magnetic frustration is anticipated because of the competition of J_1 and J_2 interactions acting between Co^{2+} spins at the A-sites. Bergman *et al.* [6] have used a Monte Carlo simulation projected on the T-J_2/J_1 plane to derive a magnetic phase diagram for

the A-site spinel antiferromagnet: As the J_2/J_1 ratio increases, the Néel point (T_N) decreases drastically, and a spin spiral (SS) state emerges above $J_2/J_1 = 1/8$. The paramagnetic-Néel (PN) and paramagnetic-SS (PSS) phase boundaries meet at the Lifshitz point (LP), and the SS phase penetrates below the Néel phase as a Néel-SS (NSS) boundary, which terminates at the quantum critical point (QCP) of $J_2/J_1 = 1/8$. Plausibly, the A-site spinel antiferromagnet $CoAl_2O_4$ realizes a Néel state in the vicinity of $J_2/J_1 = 1/8$ [6, 7, 8]. Consequently, the Néel transition temperature T_N is greatly reduced due to the degree of magnetic frustration. Remarkably, a magnetic neutron diffraction measurement [8] has revealed that a long-range AF ordering is suppressed even at $T << T_N$ for $CoAl_2O_4$. MacDougall *et al.* [8] have investigated this peculiar observation for $CoAl_2O_4$, and have revealed the formation of a fragmented AF domain structure due to the kinetically inhibited AF domain wall motion below T_N.

For the spinel oxides, distribution of the divalent (D) and trivalent (T) cations at the A- and B-sites is defined by the chemical formula $(D_{1-\eta}T_\eta)[T_{2-\eta}D_\eta]O_4$, where the parentheses and square brackets indicate the A-site and B-site occupancies, respectively, and η is the inversion parameter [5]. In our previous investigation of the A-site antiferromagnet $CoAl_2O_4$, we discovered that inversion could be tuned widely within the η range $0.02 \le \eta \le 0.153$ [9]. As shown in Fig. 1, the magnetic state is highly sensitive to the value of η. Hanashima *et al.* [10] have analyzed the magnetic states of $CoAl_2O_4$ quenched samples for inversion tuned in the range $0.0467 \le \eta \le 0.153$: they have demonstrated that a Néel-spin-glass (NSG) phase transition occurs at $\eta \sim 0.08$ (Fig. 1). Melot *et al.* [11] have studied the properties of $CoAl_{2-x}Ga_xO_4$ for $0.09 \le \eta \le 0.63$, and they have located the NSG boundary in the range $0.09 \le \eta \le 0.36$.

We therefore conducted an extensive analysis of the effect of η on magnetism of $CoAl_{2-x}Ga_xO_4$. We constructed $CoAl_{2-x}Ga_xO_4$ specimens with precise η-values and focused particularly on the vicinity of the NSG phase boundary. We discovered that the SG and Néel states separated from the paramagnetic (P) state by the phase boundaries $T_{SG}(\eta)$ and $T_N(\eta)$, respectively, in the inversion-temperature (η-T) plane; all the states met at the tricritical point $(\eta_{tc}, T_{tc}) = (0.08, 4.0\ K)$. Remarkably, for $\eta < \eta_{tc}$, the SG state penetrated below the Néel state and thereby allowed PN and NSG phase transitions. The NSG phase boundary could be traced out as an anomalous peak of the TRM relaxation rate. The slow spin dynamics detected by the TRM time course indicated the existence of an η-induced quantum phase transition and the suppression of AF long-range ordering. The latter has been observed in several previous studies [6, 7, 8, 10, 12].

II. METHODS

Polycrystalline specimens of $CoAl_{2-x}Ga_xO_4$ ($0 \le x \le 2$) were synthesized by a solid-solid reaction using appropriate amounts of CoO(4N), Al_2O_3(4N), and Ga_2O_3(4N). The mixed powder was pelletized and calcinated at 1300°C for 24 h in ordinary air and cooled to room temperature at a rate of 36°C/h. Synchrotron powder x-ray diffraction (XRD) at room temperature were carried out using two wavelengths (0.620089 Å and 0.65296 Å) on the BL15XU beam line at SPring-8 (Harima, Japan) [13] and refined the crystal structure with Rietveld analysis software, RIETAN-FP [14]. The AC and DC magnetic susceptibilities were measured with a magnetic-properties measurement system (MPMS-XL; Quantum Design) with an AC excitation field of H_{ac} = 1 Oe. The frequencies were fixed in the range 0.3–30 Hz because of the presence of significant extrinsic background signals above 300 Hz. The temperature dependence and relaxation rate of TRM were measured after field cooling (FC) with a DC excitation field of H_{FC} = 100 Oe applied at T = 70 K. After reaching the target temperature, the sample temperature was held constant for a variety of waiting periods, t_w, between 60 and 54,000 s. The applied magnetic field was then immediately reduced to zero, and the M_{TR} was recorded as a function of temperature and time. Finally, we corrected for an extrinsic paramagnetic contribution, i.e., $\chi(T)H_{res}$ produced by the residual field H_{res} less than 0.7 Oe in this work. After each isothermal relaxation measurement, H_{res} was estimated by measuring $\chi(T)H_{res}$ in the paramagnetic region (T = 70 K), where the short-range magnetic order was diminished [5,9]. For measurements of magnetization at T = 1.75 K and $B = \mu_0 H = \pm 15$ T, we used a house made high-field magnetometer and the extraction method at the Tsukuba Magnet Laboratory, National Institute for Materials Science, Japan. The specific heat of the sample was measured with a physical-properties measurement system (PPMS Dynacool; Quantum Design).

III. RESULTS

A. Inversion-temperature (η-T) phase diagram

1. Crystal structure

Figure 2 shows the XRD profile for a powdered $CoAl_{2-x}Ga_xO_4$ sample with x = 0.80. Each synthesized sample had a single-phase cubic spinel structure (space group: *Fd-3m*) that was confirmed by identifying the corresponding XRD reflection peaks (Figs. S1 and S2). We refined the crystallographic parameters by using the Rietveld method for the pseudo-ternary spinel

compound $CoAl_{2-x}Ga_xO_4$: the supplementary information (SI) describes the appropriate constraints for the refinement of cation occupancies at the A- and B-sites in the spinel lattice (Table S-I). Whereas the values for the lattice constant a and oxygen positional parameter u [Fig. 3(a)] were in accordance with those reported by Melot *et al.* [11], the A-site occupancy of Al cations, g_A(Al) [Fig. 3(b)], and the inversion parameter, η [Fig. 3(c)], were relatively small for $x < 2.0$. For the A-site occupancy of Co cations, g_A(Co), the inversion, which is defined as $\eta = 1 - g_A(\mathrm{Co})$, increased monotonically with increasing x and exhibited saturation for $x \geq 1.2$ [Fig. 3(c)]. For $CoGa_2O_4$ CG ($x = 2.0$), the observed inversion value of $\eta = 0.664(8)$ revealed the random distribution of Ga cations at both A- and B-sites [5]. Note that for $x \leq 0.8$, the A-site occupancy of Ga cations, g_A(Ga), was directly proportional to x and was described by the equation $g_A(\mathrm{Ga}) = 0.56x$ (Fig. S3). We extrapolated this relationship for $x < 0.2$ to obtain a reasonable estimate of cation occupancies and derived the crystallographic parameters listed in Table S-II. The value of u, the oxygen positional parameter, decreased linearly with increasing x for $x < 1.0$ but was relatively independent of x for $x \geq 1.0$ [Fig. 3(a)]. Empirical evidence has shown that u is a function of the ratio r_B/r_A for ternary spinel oxides, where r_A and r_B are the ionic radii of the cations occupying the A- and B-sites, respectively [15]. Indeed, the u-values obtained for $0 < x \leq 2.0$ were in reasonable agreement with the values computed using the abovementioned empirical relationship [Fig. 3(a)]. To adapt this relationship for the pseudo-ternary system $CoAl_{2-x}Ga_xO_4$, we assumed that the average cation radius, $\langle r_i \rangle$, was given by the equation $\langle r_i \rangle = g_i(\mathrm{Co})r_i(\mathrm{Co}^{2+}) + g_i(\mathrm{Al})r_i(\mathrm{Al}^{3+}) + g_i(\mathrm{Ga})r_i(\mathrm{Ga}^{3+})$, where r_i(M) is the ionic radius of the cation (M = Co, Al, or Ga) occupying the tetrahedral (i = A) and octahedral (i = B) sites. Remarkably, the linear dependence of x on u for $x < 0.6$ and insensitivity of x to u for $x > 1.2$ were fairly well reproduced [Inset of Fig. 3(c) and Fig. S4]. The monotonic relationship between η and x was therefore consistent with the relationship between u and x in $CoAl_{2-x}Ga_xO_4$.

2. DC susceptibility

Figure 4(a) shows the temperature dependence of the DC susceptibility $\chi(T)$ as a function of x for $CoAl_{2-x}Ga_xO_4$ after zero-field cooling (ZFC) and FC. Similarly to the results of Melot *et al.* [11], we identified the SG phase transition based on the temperature associated with the maximum of the derivative of the magnetic susceptibility with respect to temperature $d\chi(T)/dT$, i.e. $T_{max}(d\chi/dT)$ [Fig. 4(b)]. For $CoAl_2O_4$, this temperature coincided well with the temperature associated with the maximum of C/T, i.e. $T_{max}(C/T)$, where C is specific heat [9]. At the phase

boundary, the shapes of both $\chi(T)$ and $d\chi(T)/dT$ curves changed abruptly [Figs. 4(a) and (b)]. In this case and typically in SG systems, the $\chi(T)$ measured after ZFC exhibited a cusp at $T = T_{SG}$. The bifurcation after ZFC and FC occurred at $T < T_{SG}$. In the Néel state, there was a broad maximum of $\chi(T)$ for $T > T_N$. In accordance with the values reported by Melot *et al.* [11], the effective magnetic moment p_{eff} remained nearly constant, and the Weiss temperature θ increased as the value of x increased [Fig. 4(c)]. Figure 4(d) shows $T_{max}(d\chi/dT)$ and T_{SG} as functions of x. The hysteresis loops shown in Fig. 5 for $x = 0$, 0.2, and 0.6 at $T = 1.75$ K matched exactly with those of Melot *et al.* [11]. For $x = 0.6$, a coercive field of $H_c = 2.5$ kOe was applied, and the remanent magnetization was observed to be $m_r = 0.016$ μ_B, which was comparable to $m_0 = M_{TR}(t = 0) = 9.6 \times 10^{-3}$ μ_B at $T = 2$ K.

3. Specific heat

Figure 6 shows the temperature dependence of C/T for multiple x-values. As mentioned in previous literatures [3, 5, 6], even at $x = 0$, an anomaly in specific heat at the transition is somewhat broader. In contrast, a λ-type transition is indicated for the weakly frustrated AF $CoRh_2O_4$ [3]. The trend followed the power law $C(T) \propto T^{\alpha}$ with $\alpha \sim 7/3$ [3, 5, 6] for $T < T_N$, i.e. before the Néel phase transition. Note that $T_{max}(C/T)$ corresponded with $T_{max}(d\chi/dT)$ and an anomalous point of TRM for $x < 0.05$, as can be seen below. For $x > 0.06$, $T_{max}(C/T)$ was slightly higher than T_{SG}, and the peak of $C(T)/T$ vs. T became broader with increasing values of x (Fig. 6). Such discrepancies between T_{SG} and $T_{max}(C/T)$ have often been observed in SG compounds [5, 9].

4. TRM

TRM is a unique probe for characterizing the magnetic state and identifying phase transitions, particularly anomalies at the AF and SG phase boundaries [3, 5]. In this subsection, we describe the magnetic phase diagram obtained using measurements of dynamic and quasi-static features of TRM. Examination of the $x(\eta)$-T plane revealed that the phase boundaries determined from the TRM measurements corresponded partially with those indicated using the DC-AC susceptibilities and specific heat [Fig. 4(d)]. Such verifications are necessary to investigate the anomalous magnetic behavior of $CoAl_2O_4$ that is expected to result from magnetic frustration and inversion. Figures 7(a) and (b) show the temperature dependence of TRM intensity, $M_{TR}(T)$, and the derivative with respect to temperature of TRM,

$(1/M_{TR})(dM_{TR}/dT)$. The exponential decay of M_{TR} ceased for temperatures even slightly above the transition [Fig. 8(a)]. Between t_i = 300 and t_f = 6,300 s, the relaxation rate $\Delta M_{TR}/M_{TR} = [M_{TR}(t_f) - M_{TR}(t_i)]/M_{TR}(t_i)$ shows a sharp peak at the magnetic transition [Fig. 8(b)], especially, an intense peak at the SG transition and an Arrhenius type decay $\Delta M_{TR}/M_{TR} \propto \exp(-\Delta E/k_B T)$ observed below T_{SG} where ΔE and k_B are the activation energy and Boltzmann's constant, respectively [5]. The temperature derivative and relaxation rate curves were used in a complementary manner; the former detects both AF and SG phase transitions, whereas the latter is highly sensitive to the SG phase transition. Figures 9(a) and (b) show contour images of $(1/M_{TR})(dM_{TR}/dT)$ and $-(\Delta M_{TR}/M_{TR})/2$ in the $x(\eta)$-T plane. It should be emphasized that for $\eta < \eta_{tc} = 0.08$ [corresponding to $x = 0.06$ in the inset of Fig. 3(c)], where T_N and T_{SG} meet [Fig. 9(b)], there is an obvious peak of $\Delta M_{TR}/M_{TR}$ at x = 0.04 to 0.05 at temperatures below 4.0 K. The peak temperature $T_{max}(\Delta M_{TR}/M_{TR})$ decreased, and the peak broadened as x decreased below 0.06 [Fig. 9(b)]. A low-temperature upturn of the relaxation rate was observed for $x < 0.04$; this upturn suggests that it is possible to extrapolate the trend for $T_{max}(\Delta M_{TR}/M_{TR})$ to low temperatures below 2 K. If we assume a Debye-type TRM relaxation, $M_{TR}(t) = m_0\exp(-t/\tau_D)$ (i.e., $\Delta M_{TR}(t)/M_{TR}(0) \propto 1/\tau_D$), the low-temperature upturn corresponds qualitatively to an enhancement in the relaxation rate $1/\tau$ at $T << T_N$ for $x = 0$ ($CoAl_2O_4$) with $\eta = 0.055$ [3].

5. AC susceptibility

To confirm the realization of the SG state in the vicinity of the NSG boundary (i.e., for $\eta < \eta_{tc}$) suggested by the $\chi(T)$ and TRM measurements [Fig. 9(b)], we investigated the AC magnetic susceptibility $\chi'(T)$ for $x \leq 0.10$ (Fig. 10). The frequency dependence of $\chi'(T)$ increased with increasing η and was apparent even at low temperatures ($T < T_N$) for $0.02 \leq x \leq 0.06$. The temperature region where χ' was frequency dependent gradually expanded toward high temperatures for increasing x-values. This trend was consistent with the TRM observation that the SG state was realized at $T < T_{max}$ and $\eta < \eta_{tc}$. However, for x = 0.05, no discernable kinks were observed in the $\chi'(T)$ curve at $T \approx T_{max}(\Delta M_{TR}/M_{TR}) < T_N$ that would have enabled effective detection of the NSG phase boundary (Fig. 10). In contrast, as discussed below, the magnetic dynamics detected through TRM were much more sensitive to the NSG transition, and they revealed important information about the η-dependent magnetic properties of $CoAl_2O_4$.

B. Magnetic dynamics

1. TRM at phase boundaries

Before identifying the NSG boundary in the η-*T* plane for $CoAl_{2-x}Ga_xO_4$, we first discuss formation of the CG state at $T < T_N$ in the vicinity of the NSG boundary and the tricritical point. We analyzed the temporal evolution of TRM relaxation based on Weron's generalized probabilistic function. The Weron function $\phi_W(t)$ for universal relaxation is based on a purely stochastic theory and is defined as

$$\phi_W = \left[1 + k\left(\frac{t}{\tau}\right)^{\beta}\right]^{-1/k}, \quad (1)$$

where $k > 0$ is the interaction parameter, and $\beta \in (0,1)$ is the scaling parameter defining the general relation ($\tau = v^{1/\beta}$) for the relaxation time τ of particles in a volume v [16]. The k-parameter relates to the collective nature of the interactions and t_w. For $k \to 0$ and $k \to \infty$, Eq. (1) asymptotically approaches the stretched exponential and logarithmic functions, respectively. The β-parameter relates to the fractal geometry and nature of relaxation. As shown in Figs. 11(a) and (b), the Weron function reproduced the experimentally obtained $M_{TR}(t)$ and a derivative with respect to logarithmic time of M_{TR}, $S(t)$, with quantitatively reasonable values. The logarithmic time derivative $S(t)$ is defined as

$$S(t) = -d\left(\frac{M_{TR}}{H_{FC}}\right)/d\ln t, \quad (2)$$

which is a bell-shaped curve with a broad maximum at $t = \tau$, as shown in Fig. 11(b). Interestingly, $S(t)$ provides us approximately the density of the relaxation time $t = \tau$ [2]. For an SG sample with $x = 0.08$ and $T_{SG} = 3.8$ K, the maximum point of $S(t)$ corresponding to $t = \tau$, and the peak width broadened significantly with decreasing temperature [Fig. 11(b)]. Numerically, it was easily demonstrated that the parameters k and β in the Weron function (Eq. 1) strongly affected the τ-density. Both an increment in k and decrement in β contribute to broadening of an $S(t)$ peak profile and gradually lead to a logarithmic relaxation [$M_{TR}(t) \propto \ln t$]. For $x = 0.08$, the $S(t)$ profile broadened with increasing k and decreasing temperature [Fig. 11(b)]. We used Eq. (1) to extract the macroscopic parameters τ, k, and β at various x-values and temperatures from the isothermal temporal evolution of $M_{TR}(t, T)$. Figures 12(a) and (b) show relaxation time τ, for $0 \le x \le 0.10$ ($0.055 \le \eta \le 0.10$), as a function of the reduced

reciprocal temperatures T_N/T and T_{SG}/T, respectively. In the Néel state, for $x = 0$ and 0.02, there was a clear decrement of τ with decreasing temperature. The negative gradient of τ with the inverse of temperature was consistent with the observation of an upturn in the relaxation rate at low temperatures [Fig. 8(b)]. For the $CoGa_2O_4$ CG and disorder-free $CoRh_2O_4$, τ seemed to obey an Arrhenius law $\tau(T) \propto \exp(E_a/k_BT)$, where E_a is an activation energy comparable with k_BT_i (i = N or SG) as mentioned previously [3].

Figures 13(a) and (b) show the variation of k with the reduced temperatures T/T_N and T/T_{SG}, respectively, for CoM_2O_4 (M = Al and Ga). After the TRM measurements described in subsection A4 had been made for $x = 0.04$ and 0.05, the magnetic states at $T > T_N$, $T_N > T > T_{max}$, and $T < T_{max}$ were identified as P, long-range ordered AF, and SG, respectively [Fig. 9(b)]. On the basis of the relaxation parameters, we evaluated the magnetic transitions and states separated by the NSG phase boundary as well as those in the vicinity of the tricritical point for $0 \le x \le 0.10$. For $T < T_{SG} = 3.9$ K and $x = 0.10$, the sample developed an SG state. There was a sharp minimum of the relaxation time $\tau(T)$ at $T = T_{SG}$. The relaxation time increased as the temperature decreased below T_{SG} in accord with an Arrhenius law [Fig. 12(b)]. The interaction parameter $k(T)$ decreased with increasing temperature (similarly to the trend of the $CoGa_2O_4$ CG), reached a minimum at around $T \sim T_{SG}$, and increased rapidly for $T > T_{SG}$ [Fig. 13(b)]. This pattern of $k(T)$ was maintained qualitatively for $x = 0.04$ and 0.05 as well, although the value of $k(T_{max})$ increased systematically with decreasing η. In the intermediate state for $T_{max} < T < T_N$, the value of $k(T)$ increased and was comparable to that of the $CoRh_2O_4$ antiferromagnet for T slightly below T_N. Based on the work of Tsallis [17] on non-extensive statistical mechanics, we know that the interaction parameter is directly related to a non-extensive parameter q via a simple equation, $k = (q - 1)/(2 - q)$ [18]. In previous studies, the q for SG samples, metallic systems $Cu_{1-x}Mn_x$ and $Au_{1-x}Fe_x$ [19] and $CoGa_2O_4$ [5], were experimentally obtained as a function of temperature and exhibited the following characteristics: for $T/T_{SG} << 1$, $q(T) \rightarrow 2$ (asymptotically) and $q(T_{SG}) = 5/3$; for $T/T_{SG} >> 1$, $q(T) = 0$. As shown in Fig. 14, the $q(T)$ for $x = 2$ ($CoGa_2O_4$ CG) exhibited similar features. However, for $x = 0.06$ and 0.10, there was a broad minimum of $q(T)$ for $T < T_{SG}$, and $q(T)$ increased rapidly for $T > T_{SG}$. This recovery of q and k at high temperatures, which was observed for $0.04 \le x \le 0.10$ [Fig. 13(b)], implies that an AF correlation is maintained for $T > T_{max}$ or $T > T_{SG}$. Note that there was an abrupt increase of $\beta(T)$ in the vicinity of T_{SG} for the SG states of $x = 0.06$ and 0.10 ($\eta > \eta_{tc}$). In addition, $\beta(T)$ was constant for $T < T_{SG}$. The specific temperature variations of $k(T)$ and $\beta(T)$ provided indications

of whether and where an SG transition had occurred. The fact that similar behavior of $k(T)$ and $\beta(T)$ were also observed at $x = 0.04$ and 0.05 ($\eta < \eta_{tc}$) strongly suggests that the NSG phase transition occurred at T_{max}.

2. Ageing

We extrapolated the phase boundary temperature $T_{max}(\Delta M_{TR}/M_{TR})$ for $x \sim 0.03$ and $T = 2$ K [Fig. 9(b)]. In this subsection, we analyze the ageing behavior (i.e., the t_w-dependence of TRM relaxation), which is often investigated for $T < T_{SG}$ in SG systems [2, 20]. Figure 15(a) shows the t_w-dependence of τ computed by fitting the relaxation curve to Eq. (1). For $CoAl_{2-x}Ga_xO_4$, $\tau(t_w)$ curves followed an empirical relation $\tau = \tau_a + (\tau_b^{-1} + t_w^{-1})^{-1}$, where τ_a and τ_b are constants; τ_b is a characteristic time that represents the upper limit to the time to observe ageing behavior. For $\tau_b >> t_w$, the above relation can be simplified to $\tau = \tau_a + t_w$. In the SG state of the $x = 0.04$ sample, τ followed the above simplified relationship, where τ_a was related to the effective time (t_{cool}) required to cool the sample from $T > T_N$ or T_{SG} to the target temperature by application of a magnetic field with an H_{FC} equal to 100 Oe. Based on the TRM protocol used in this work, we estimated t_{cool} to be less than 300 s. This time was much smaller than $\tau_a = 3{,}000$ s at $T = 2$ K (with $T/T_{SG} \approx 0.4$) for $x = 0.60$. Consequently, because $\tau >> t_w = 300$ s, the experimentally obtained value of τ reflected the magnetic and thermodynamic characteristics of the sample. In contrast, for $t_w >> \tau_a$, $\tau(t_w)$ asymptotically approached the line $\tau = t_w$ and thereby confirmed the ageing behavior of TRM relaxation [Fig. 15(a)]. The t_w-dependence of τ for $x = 0.03$ at $T = 2$ K was comparable to that for $x = 0.04$, although the dependence for $x \leq 0.02$ was rather weak. For $x = 0.02$, the $\tau(t_w)$ curve crossed the $\tau = t_w$ line at $t_w = 2{,}000$ s. This discrepancy between the $x = 0.02$ and 0.03 cases might suggest that the NSG phase boundary coordinate located at (x, T) ~ (0.03, 2.0 K), which matched with the extrapolated value for $T_{max}(\Delta M_{TR}/M_{TR})$ [Fig. 9(b)]. Both $k(t_w)$ and $\beta(t_w)$ decreased with increasing t_w. The slopes of $k(t_w)$ and $\beta(t_w)$ with respect to $\log(t_w)$ were observed to strongly depend on η [Figs. 15(b) and (c)].

IV. DISCUSSION AND CONCLUSIONS

By measuring the DC and AC magnetic susceptibilities, TRM, and specific heat, we demonstrated that an inversion-induced NSG transition occurs in $CoAl_{2-x}Ga_xO_4$. We constructed a magnetic phase diagram in the inversion-temperature (η-T) plane for $0.055 \leq \eta \leq$

0.10 and down to T = 2 K. The P, Néel (AF), and SG states met at the tricritical point (η_{tc}, T_{tc}) = (0.08, 4.0 K). We used TRM measurements to identify the low-temperature branch of the magnetic phase boundary, which we expected to be the NSG boundary, and we also verified the identification through an analysis of AC susceptibility. The relaxation rate $\Delta M_{TR}/M_{TR}$ exhibited anomalous peaks that could be associated with the PN, PSG, and NSG boundaries. Remarkably, the SG state penetrated into the Néel state for $\eta < \eta_{tc}$ and established an NSG phase boundary that was extrapolated as $\eta \sim 0.068$ ($x \sim 0.03$) at T = 2 K [Fig. 9(b)]. To rigorously confirm the presence of the NSG phase boundary at T = 2 K, we analyzed the relaxation time τ and the stochastic parameters k and β as functions of t_w and η [Fig. 15 and Figs. 16(b)–(d)].

We observed that at T = 2 K, the value of τ for x = 0.02 (η = 0.064) and x = 0.03 (η = 0.068) exhibited a weak and strong dependence, respectively, on t_w [Fig. 15(a)]. For $x \geq 0.03$, the value of τ followed a simplified empirical law, $\tau(t_w) = \tau_a + t_w$, and it asymptotically approached the $\tau = t_w$ line for $t_w >> \tau_a$ (n.b., τ_a is a constant that depends on the TRM measurement protocol) [21]. This strong dependence of TRM relaxation on t_w for $x \geq 0.03$ implied the realization of an SG state [2]. For x = 0.02, we observed a peculiar two-step crossover t_w-dependence of τ due to crucial reductions in τ_a and τ_b in the vicinity of the NSG phase boundary. To verify the realization of this two-step crossover, further investigation of the TRM relaxation will be required for T > 2 K. Both the stochastic parameters k and β decreased with increasing t_w. The decrement in β with increasing t_w has been previously reported for the short-range Ising SG system [21], although, in that study, β was extracted from the relaxation curves using a stretched exponential.

The relaxation parameters exhibited certain anomalous behaviors as functions of inversion. The k parameter increased with decreasing η, with a particularly steep increment for $\eta < 0.08$. At the same time, the β and $1/\tau$ parameters showed significant enhancements for $0.02 \leq x \leq 0.03$ ($0.064 \leq \eta \leq 0.068$) [Fig. 16(c) and (d)]; this anomalous region corresponds to the boundary that defined the strong or weak t_w-dependence of τ [Fig. 15(a)]. We also observed enhancements in $1/\tau$ and β in the vicinity of the thermally induced PSG phase transition [Figs. 12(b) and 13(c)]. The absence of anomalies in specific heat measurements at T_{max} was due to the low magnetic entropy released at the NSG phase boundary compared to the PN and PSG phase boundaries.

Together with the anomalous value of η (0.066) at T = 2 K denoted as η_{age}, the linear extrapolation of T_{max} ($\Delta M_{TR}/M_{TR}$) with η [Fig. 16(a)] enabled us to estimate a zero-temperature boundary at η = 0.050(6). For $x \leq 0.02$ (η = 0.064), both $\Delta M_{TR}/M_{TR}$ and $1/\tau$ increased with decreasing temperature [Figs. 8(b) and 12(a)]. These increases indicate a proximity to the NSG transition at low temperatures. We therefore postulate that the NSG boundary could be extrapolated for T < 2 K and that an NSG QCP is located at η_{qc} = 0.050(6). Assuming the existence of this QCP, we examined the η-(J_2/J_1) plane for $\eta < \eta_{tc}$ by taking advantage of the following observations. We noticed that the $k(T/T_{SG})$ curve for $0.04 \leq x \leq 0.10$ gradually approached the curve for a $CoGa_2O_4$ CG [5] and canonical SGs [19]. Therefore, we speculate that for $\eta < \eta_{tc}$, the SG state coexists with the Néel state, even below the NSG boundary (for $T < T_{NSG}$). In other words, the transition at the NSG phase boundary could be a first-order transition. This argument follows from the existence of an LP where the P, uniform, and modulated spin states meet [22]. The Landau free energy allows the construction of a phase diagram containing a QCP and LP. Depending on whether the order parameter is a scalar or vector, the transition from a uniform phase to a modulated spin phase at the phase boundary between the QCP and LP would be a first-order or second-order transition, respectively. This situation has occurred on the J_2/J_1-T plane of an A-site spinel magnet [6]. Our experimentally obtained η-T phase diagram is quite similar to the theoretically predicted J_2/J_1-T phase diagram for an A-site antiferromagnet. However, the CG state that was realized in the η-T plane was unlike the spatially modulated spin spiral (SS) state realized in the J_2/J_1-T plane. We therefore speculate that the AF fragments could be quenched from the Néel state and frozen in a metastable SG state. This work contributes to the understanding of the controversial magnetic ground state of a slightly inverted A-site spinel magnet $CoAl_2O_4$, and it paves the way for further investigations, such as the construction of an η-J_2/J_1 phase diagram for $T << T_{tc}$. The speculations based on the findings revealed in this study were led from mainly the macroscopic observations down to T = 2 K, and therefore, to confirm the speculations, especially, the realization of the NSG-QCP in a slightly inverted $CoAl_2O_4$, both macroscopic and microscopic investigations are required to conduct at low temperatures below 2 K.

ACKNOWLEDGEMENTS

This work was supported by World Premier International Research Center Initiative (WPI). This work was partially supported by a Grant-in-Aid for Scientific Research (KAKENHI Grants

No. 25246013, No. 16K13999, No. 21H01637, No. 19H05790, No. 19H05819, and No. 21F21322) and the Research Institute for Science and Technology of Tokyo Denki University (Grant No. Q23K-01). The synchrotron radiation experiments were performed using the BL15XU beam line at SPring-8 with the approval of the Japan Synchrotron Radiation Research Institute (Grants No. 2015B4505, 2016B4505, and 2018A4507).

References

[1] R. F. Butler, Magnetic Domains to Geologic Terranes (Blackwell Science Inc., Boston, 1991).

[2] E. Vincent, "Ageing, Rejuvenation and Memory: The Example of Spin-Glasses", in *Ageing and the Glass Transition*, ed. M. Henkel, M. Pleimling, and P. Sanctuary (Springer Berlin Heidelberg, 2007).

[3] T. Naka, T. Nakane, J. Valenta, H. Mamiya, S. Ishii, M. Nakayama, H. Abe, T. Togashi, and T. Uchikoshi, J. Phys. Commun. **6**, 055001 (2022).

[4] T. Naka, J. Valenta, J. Kaštil, M. Míšek, J. Prchal, V. Sechovský, H. Abe, T. Nakane, M. Nakayama and T. Uchikoshi, Mater. Res. Express **7**, 056105 (2020).

[5] T. Naka, T. Nakane, S. Ishii, M. Nakayama, A. Ohmura, F. Ishikawa, A. de Visser, H. Abe and T. Uchikoshi, Phys. Rev. B **103**, 224408 (2021).

[6] D. Bergman, J. Alicea, E. Gull, S. Trebst, and L. Balents, Nature Phys. **3**, 487 (2007).

[7] O. Zaharko, S. Toth, O. Sendetskyi, A. Cervellino, A. Wolter-Giraud, T. Dey, A. Maljuk, and V. Tsurkan, Phys. Rev. B **90**, 134416 (2014).

[8] G. J. MacDougall, A. A. Aczel, Yixi Su, W. Schweika, E. Faulhaber, A. Schneidewind, A. D. Christianson, J. L. Zarestky, H. D. Zhou, D. Mandrus, and S. E. Nagler, Phys. Rev. B, **94**, 184422 (2016).

[9] T. Naka, K. Sato, Y. Matsushita, N. Terada, S. Ishii, T. Nakane, M. Taguchi, M. Nakayama, T. Hashishin, S. Ohara, S. Takami and A. Matsushita, Phys. Rev. B, **91**, 224412 (2015).

[10] K. Hanashima, Y. Kodama, D. Akahoshi, C. Kanadani, and T. Saito, J. Phys. Soc. Jpn. **82**, 024702 (2013).

[11] B. C. Melot, K. Page, R. Seshadri, E. M. Stoudenmire, L.Balents, D. L. Bergman, and T. Proffen, Phys. Rev. B **80**, 104420 (2009).

[12] Somnath Ghara, N. V. Ter-Oganessian, A. Sundaresan, Phys.Rev. B, **95**, 094404 (2017).

[13] E. Nishibori, M. Takata, K. Kato, M. Sakata, Y. Kubota, S. Aoyagi, Y. Kuroiwa, M. Yamakata, and N. Ikeda, Nuc. Instrum. Methods Phys. Res. A, **467-468**, 1045 (2001).

[14] F. Izumi and K. Momma, Solid. State Phenom., **130**, 15 (2007).

[15] Kurt E. Sickafus, John M. Wills and Norman W. Grimes, J. Am. Ceram. Soc., **82**, 3279–92 (1999).

[16] K. Weron, J.Phys, **3**, 9151-9162 (1991).

[17] Constantino Tsallis, Introduction to Nonextensive Statistical Mechanics (Springer, New York, USA, 2009).

[18] F. Brouers and O. Sotolongo-Costa, Europhys. Lett. **62**, 808 (2003).

[19] R. M. Pickup, R. Cywinski, C. Pappas, B. Farago, P. Fouquet, Phys. Rev. Lett., **102**, 097202 (2009).

[20] P. Granberg, L. Lundgren and P. Nordblad, J. Magn. Magn. Mater.**92**, 228 (1990).

[21] I. S. Suzuki and M. Suzuki, Phys. Rev. B **78**, 214404 (2008).

[22] P. M. Chaikin and T. C. Lubensky, Principles of condensed matter physics (Cambridge University Press, Cambridge 1997).

[23] O. Zaharko, A. Cervellino, V. Tsurkan, N. B. Christensen, and A. Loidl, Phys. Rev. B **81**, 064416 (2010).

[24] N. Tristan, J. Hemberger, A. Krimmel, H-A. Krug von Nidda, V. Tsurkan, and A. Loidl, Phys. Rev. B, **72**, 174404 (2005).

[25] T. Suzuki, H. Nagai, M. Nohara, and H. Takagi, J. Phys. Condens. Matter **19**, 145265 (2007).

[26] G. J. MacDougall, D. Gouta, J. L. Zarestky, G. Ehlers, A.Podlesnyak, M. A. McGuire, D. Mandrus, and S. E. Nagler, Proc. Natl. Acad. Sci. U.S.A. **108**, 15693 (2011).

[27] O. Zaharko, N. B. Christensen, A. Cervellino, V. Tsurkan, A. Maljuk, U. Stuhr, C. Niedermayer, F.Yokaichiya, D. N. Argyriou, M. Boehm, A. Loidl, Phys. Rev. B **84**, 094403 (2011); A. Maljuk, V. Tsurkan, V. Zestrea, O. Zaharko, A. Cerellino, A. Loidl, and D.N.Argyriou, J. Cryst. Growth **311**, 3997 (2009).

[28] B. Roy, Abhishek Pandey, Q. Zhang, T. W. Heitmann, D. Vaknin, D. C. Johnston, and Y. Furukawa, Phys. Rev. B **88**,174415 (2013).

[29] M. Iakovleva, E. Vavilova, H.-J. Grafe, S. Zimmermann, A. Alfonsov, H. Luetkens, H.-H. Klauss, A. Maljuk, S. Wurmehl, B. Buchner, and V. Kataev, Phys. Rev. B **91**, 144419 (2015).

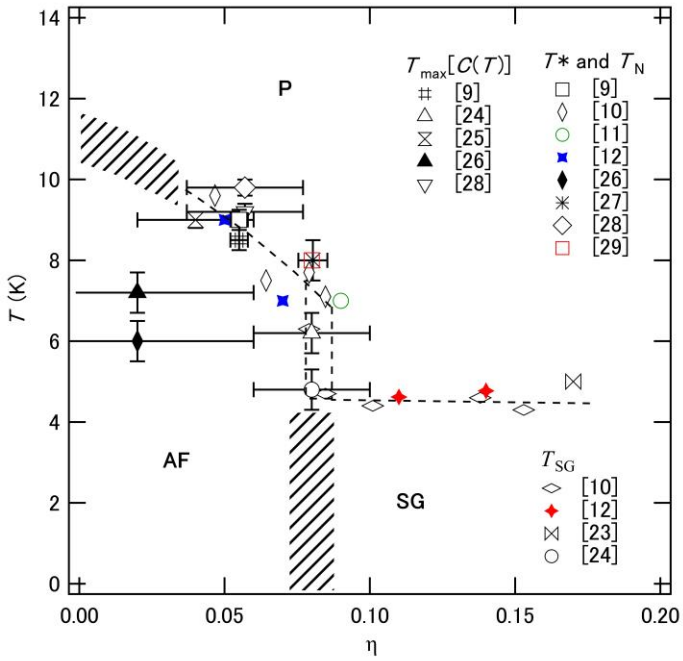

FIG. 1. Inversion-temperature (η-T) phase diagram for $CoAl_2O_4$ based on multiple studies since 2005 [9] and including plots for recently reported data points [11,12,29]. Transition temperatures denoted by $T_N(T^*)$, T_{SG}, and $T_{max}[C(T)]$ were determined by measurements of magnetic susceptibility [9–12,23,24,26,27], NMR [28,29], and specific heat [9,24–26,28]. Dashed lines and hashed areas aid visualization. P, AF and SG denote paramagnetic, antiferromagnetic (Néel) and spin-glass states, respectively. The figure was originally published in Ref. 9, with the addition of several data points recently reported [11,12,29].

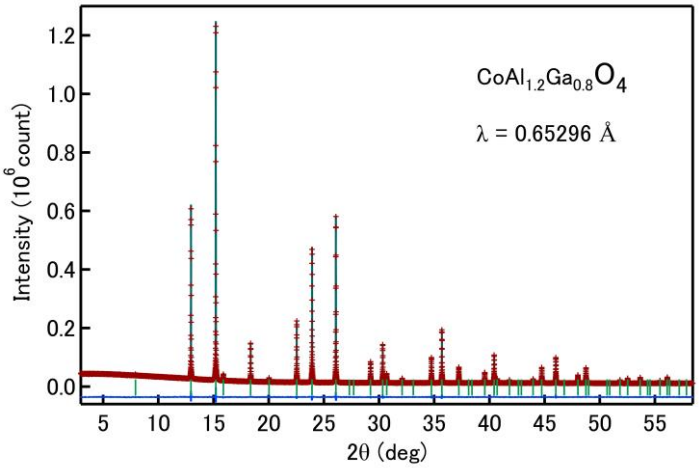

FIG. 2. XRD profile for $CoAl_{1.2}Ga_{0.8}O_4$. The vertical green lines show the positions of the Bragg reflections. The blue trace indicates the difference between the observed and computed intensities.

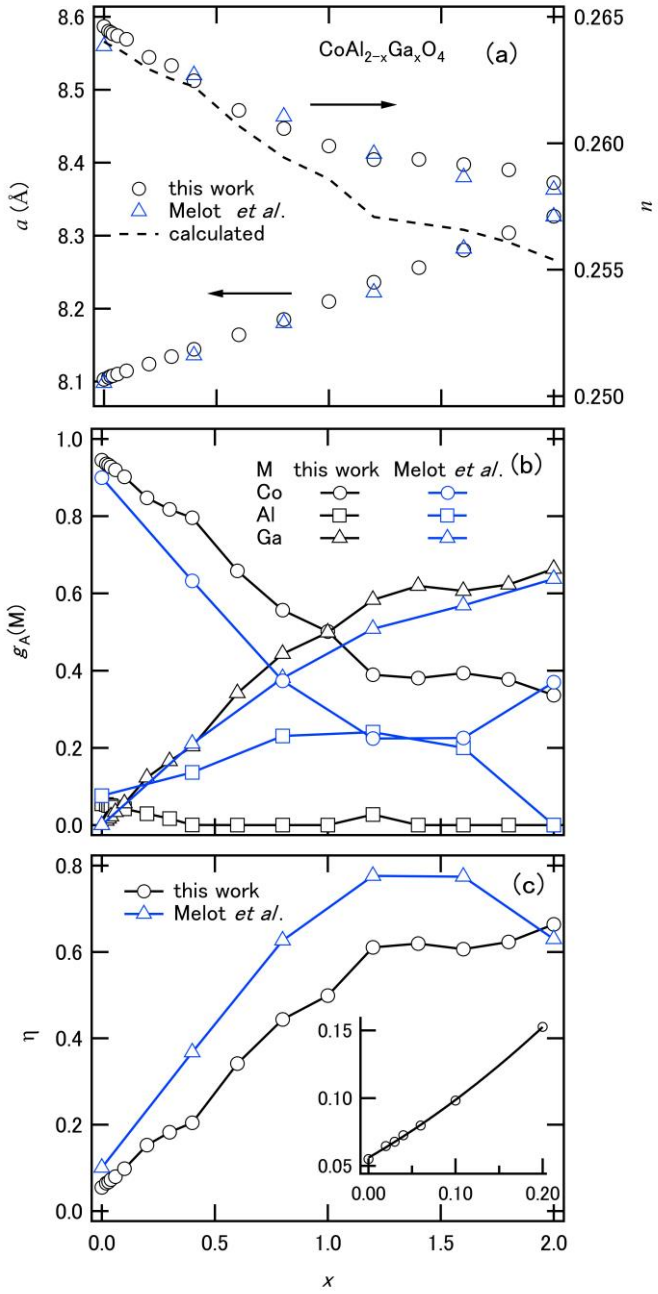

FIG. 3. Variations of (a) lattice constant a and oxygen positional parameter u, (b) A-site occupancies of Co, Al, and Ga ions, and (c) inversion parameter η as functions of x for $CoAl_{2-x}Ga_xO_4$. Dashed line in (a) represents the u-parameter computed based on the empirical relation formulated in a previous work [15]. Inset in (c) shows $\eta(x)$ in the range of $0 \leq x \leq 0.2$, where the solid line was obtained by least squares (also see SI).

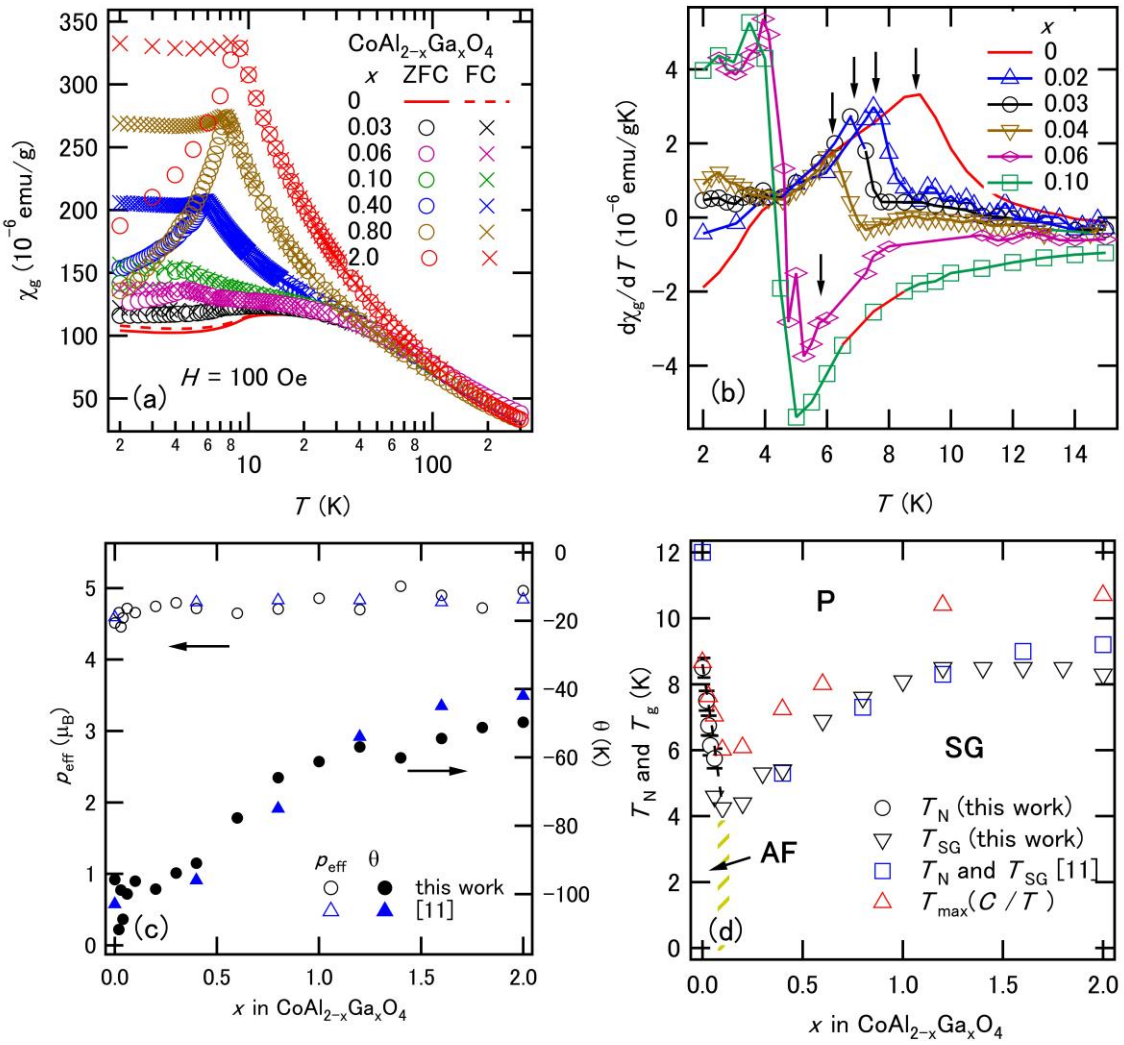

FIG. 4. (a) DC–magnetic susceptibility as a function of temperature for $CoAl_{2-x}Ga_xO_4$, measured at H = 0.1 kOe after zero-field cooling (ZFC) and field cooling (FC). Data points for x = 0 and 2.0 are taken from previous works [5,9]. (b) Temperature derivative of susceptibility $d\chi_g/dT$ as a function of temperature; the arrows indicate the magnetic transition temperature T_N. (c) Effective magnetic moment p_{eff} and Weiss temperature θ as functions of x. (d) Temperature-composition (x – T) phase diagram. The hashed area around x = 0.06 represents the phase boundary between the Néel (antiferromagnetic, AF) and spin glass (SG) states. Previously reported values [11] are plotted in (c) and (d) for comparison.

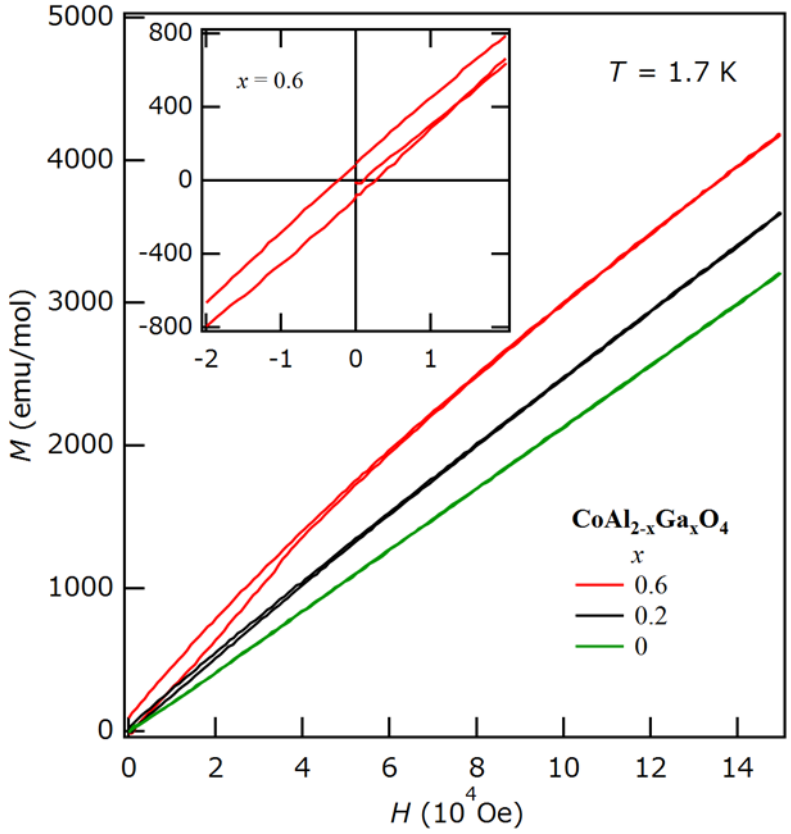

FIG. 5. Hysteresis loops for $x = 0$, 0.2, and 0.6 measured at $T = 1.7$ K for $CoAl_{2-x}Ga_xO_4$. Inset shows the minimized view for $x = 0.6$.

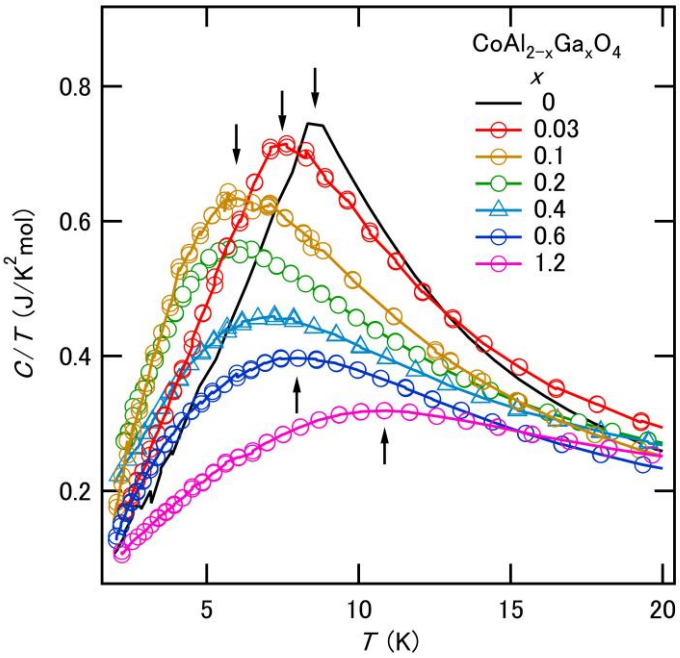

FIG. 6. Temperature-scaled specific heat as function of temperature for x = 0.03, 0.1, 0.2, 0.4, 0.6, and 1.2. The solid black line represents $C(T)/T$ for $CoAl_2O_4$ taken from previous work [9]. Arrows indicate maximum points of $C(T)/T$ at various gallium compositions.

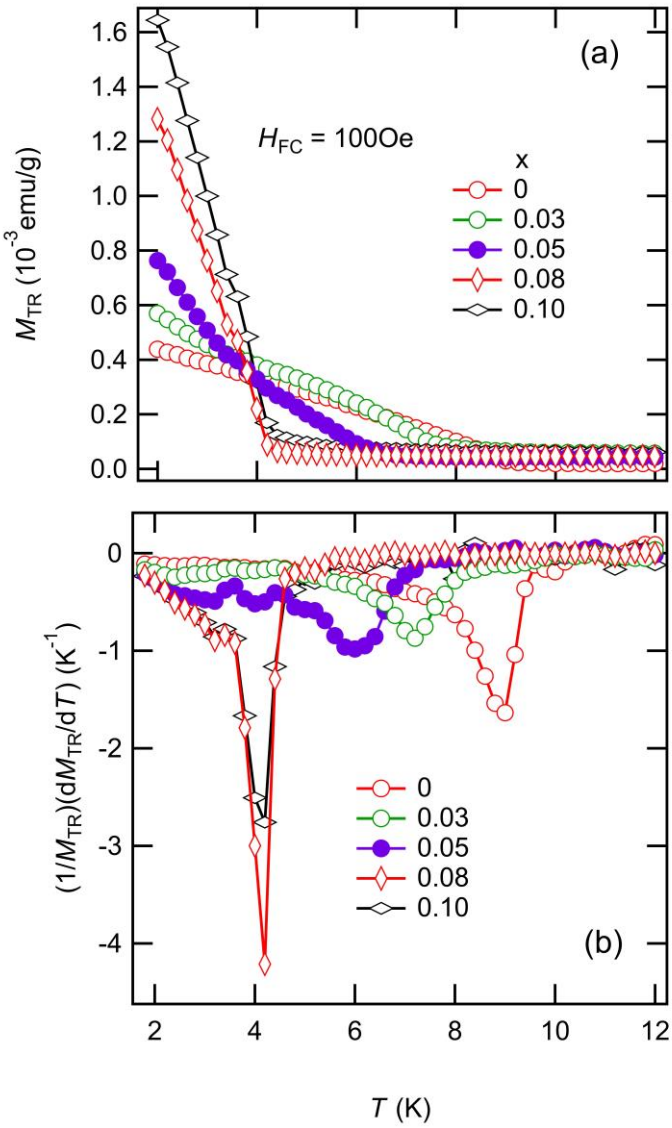

FIG. 7. Temperature dependence of (a) thermoremanent magnetization intensity $M_{TR}(T)$ and (b) the derivative of its natural logarithm with respect to temperature $(dM_{TR}/dT)/M_{TR}$ for $0 \leq x \leq 0.10$. An activation field H_{FC} = 100 Oe was applied during field cooling prior to the isothermal measurement of thermoremanent magnetization.

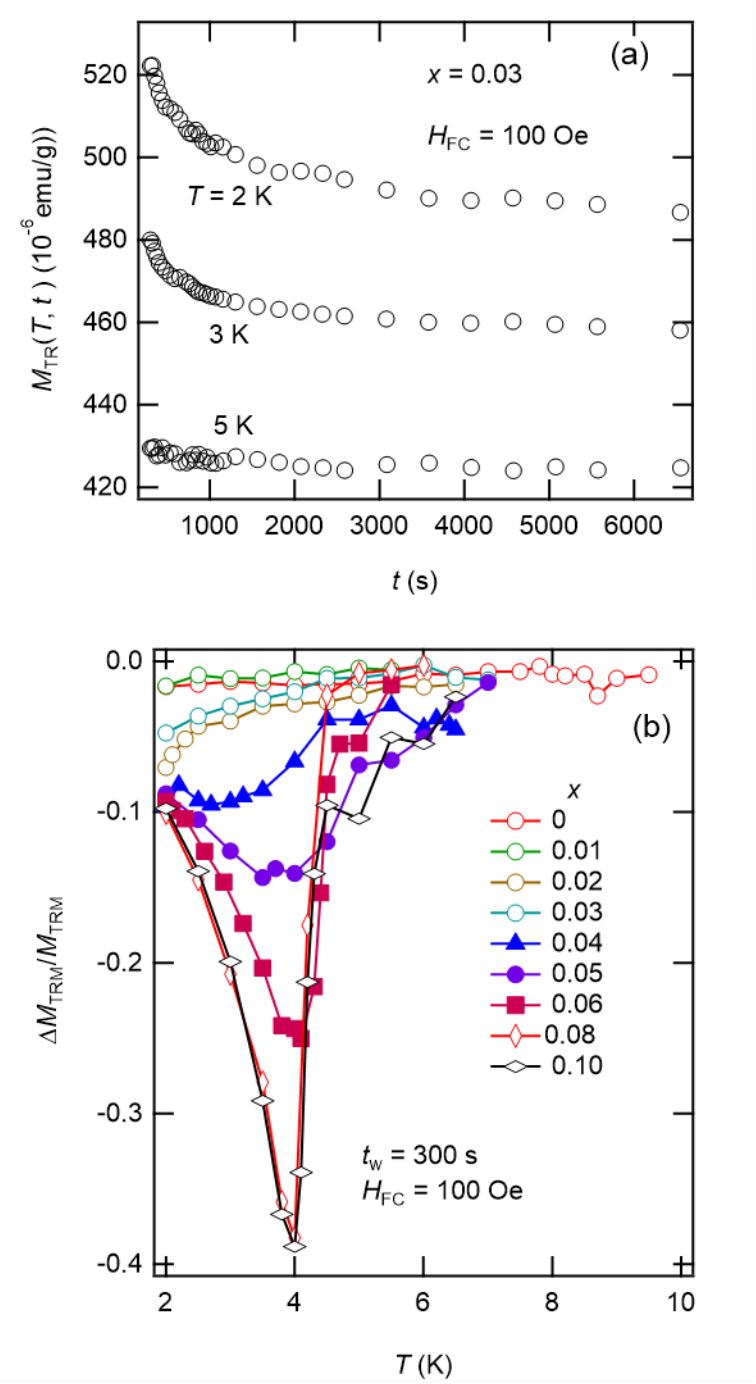

FIG. 8. (a) Isothermal time evolution of thermoremanent magnetization intensity M_{TR} at various temperatures for $x = 0.03$. (b)Temperature dependence of relaxation rate $\Delta M_{TR}/M_{TR} = [M_{TR}(t_f) - M_{TR}(t_i)]/M_{TR}(t_i)$ for $0 \leq x \leq 0.10$ with $t_i = 300$ and $t_f = 6300$ s.

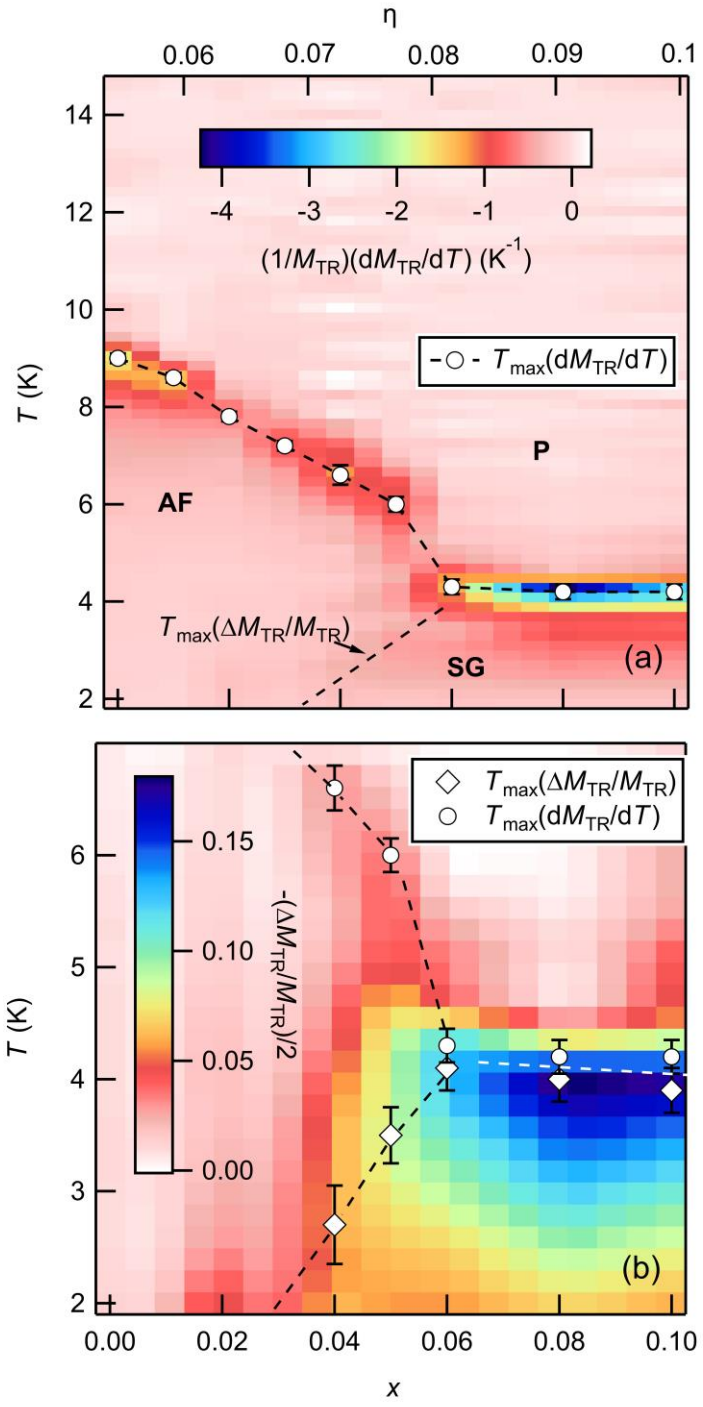

FIG. 9. Contour images of (a) the derivative with respect to temperature of thermoremanent magnetization intensity $(1/M_{TR})(dM_{TR}/dT)$ and (b), $-(\Delta M_{TR}/M_{TR})/2$ (relaxation rate scaled by the factor of –1/2 for plotting convenience) on the $x(\eta)$-T plane.

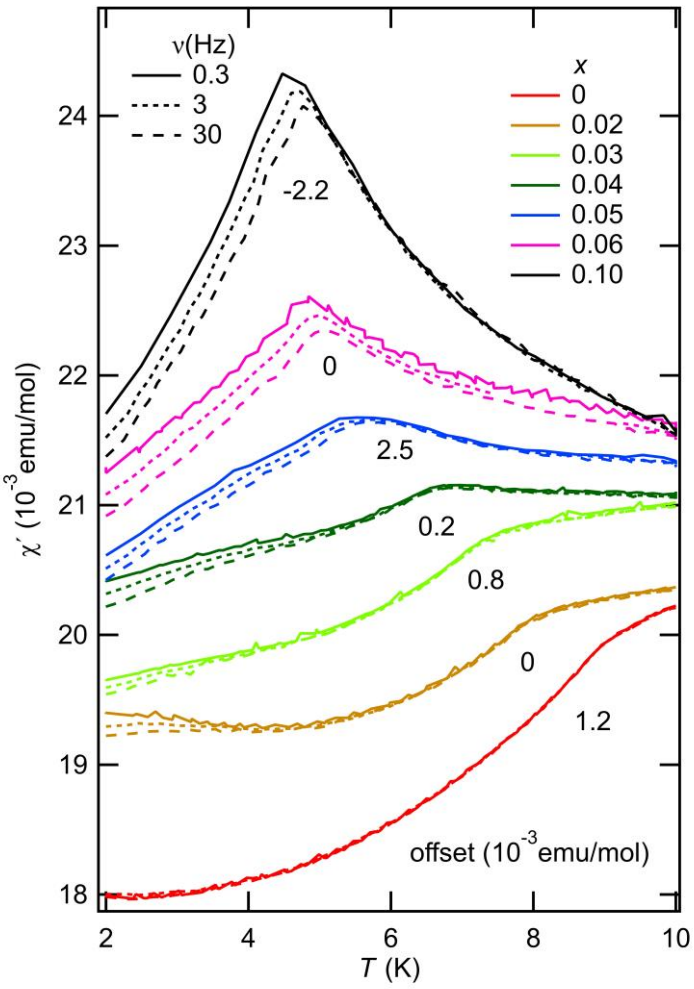

FIG.10. Temperature dependence of the real component of the alternating current susceptibility $\chi'(T)$ for $0 \leq x \leq 0.10$ at various frequencies.

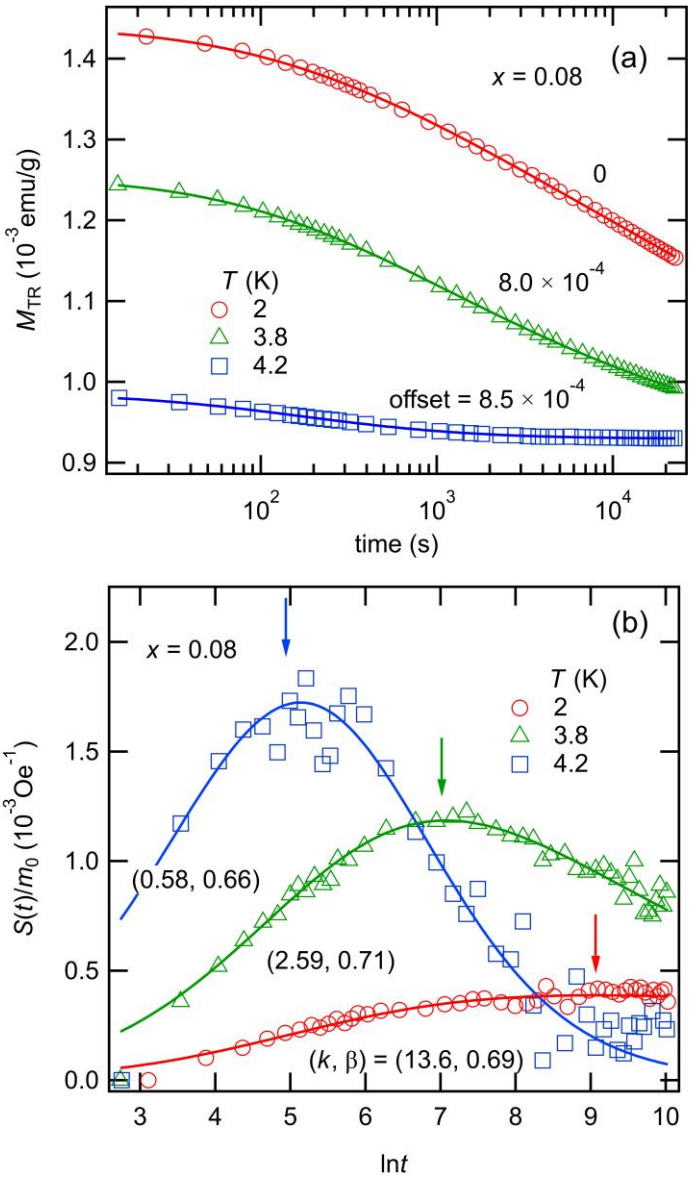

FIG. 11. (a) Isothermal relaxation of thermoremanent magnetization intensity, $M_{TR}(t)$, measured at T = 2, 3.8, and 4.2 K for x = 0.08. Solid line represents a numerically fitted curve of Eq. (1). The relaxation curve is offset along the vertical axis with the value shown against each curve in the unit of emu/g to aid visualization. (b) Logarithmic time derivative of $M_{TR}(t)$, $S(t)$, scaled by $m_0 = M_{TR}(t = 0)$ as a function of logarithmic time. Solid lines represent the calculated $S(t)/m_0$ using the fitting parameters m_0, τ, k, and β. The arrows indicate the positions for $t = \tau$. Values of relaxation parameters k and β are represented in parentheses against each curve.

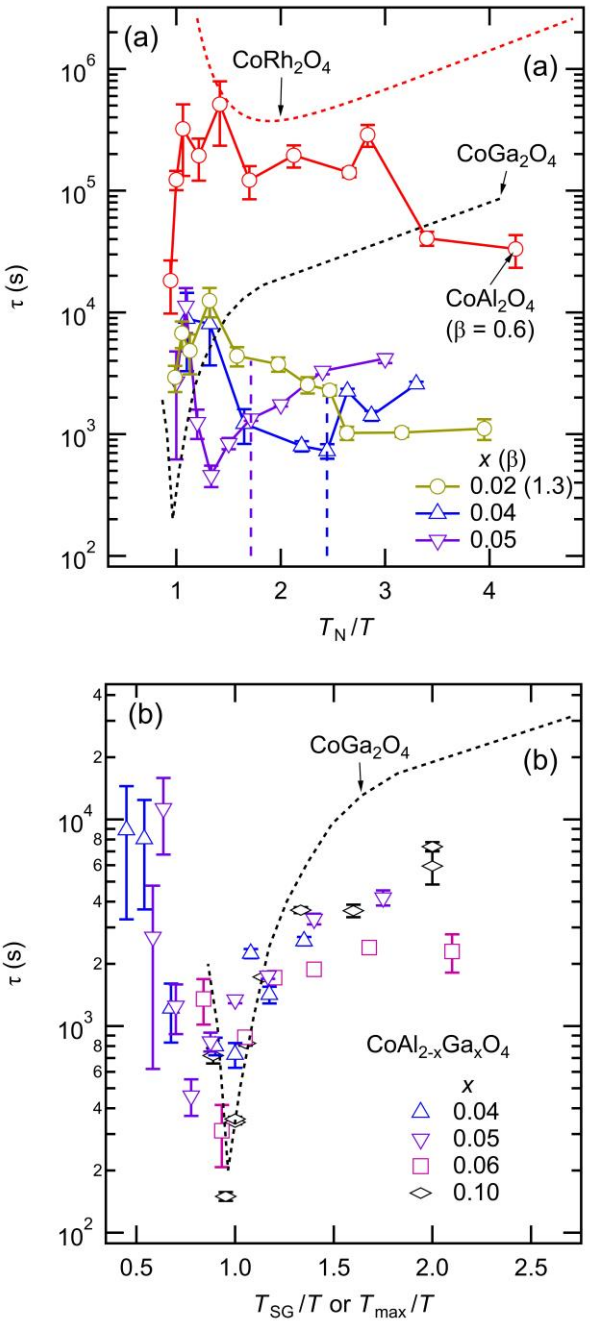

FIG. 12. Relaxation time τ as a function of the inverse of the reduced temperatures (a) T_N/T and (b) T_{SG}/T or T_{max}/T for $CoAl_{2-x}Ga_xO_4$. Here $T_{max} = T_{max}(\Delta M_{TR}/M_{TR})$. Note that, for $x = 0.04$ and 0.05, the magnetic anomalies are indicated both at $T = T_N$ and $T_{max}(\Delta M_{TR}/M_{TR})$. Data points for CoM_2O_4 (M = Al, Ga, and Rh) are taken from previous works [3,5]. Blue and purple dashed vertical lines in (a) indicate T_{max}/T_N for $x = 0.04$ and 0.05, respectively. For $x = 0.02$, we chose $\beta = 1.3$, a value that we obtained experimentally at $T = 2$ K and $t_w = 300$ s [Fig. 16(d)].

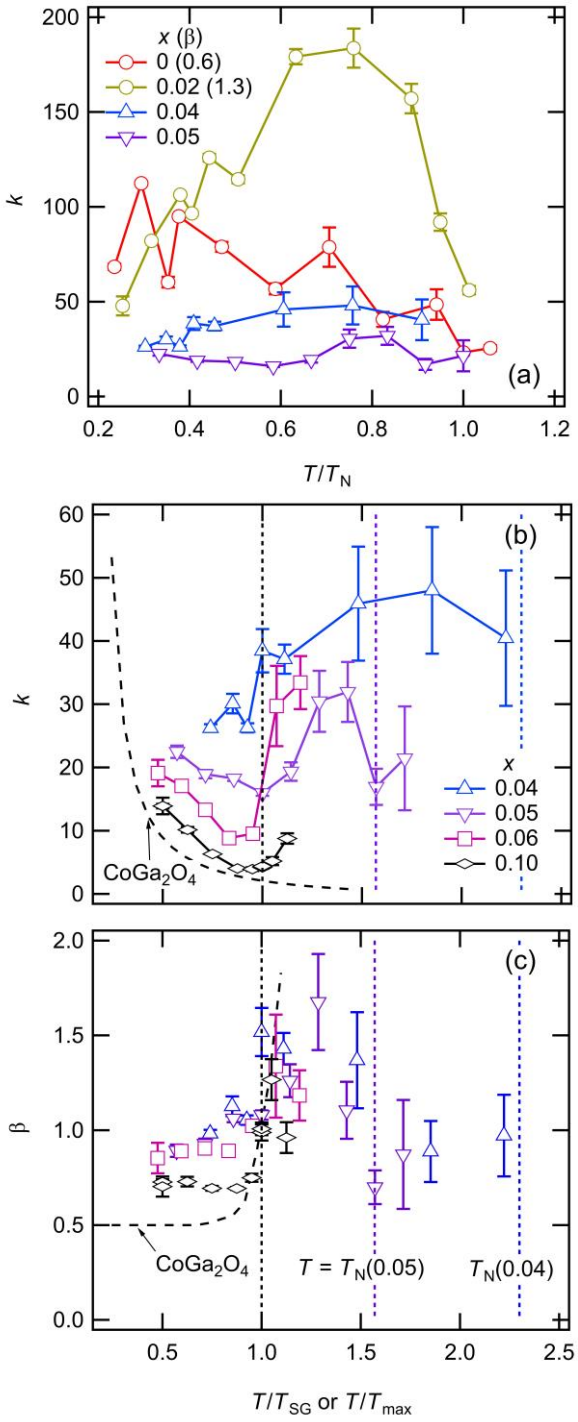

FIG. 13. Interaction parameter k as a function of reduced temperatures (a) T/T_N and (b) T/T_{SG} or T/T_{max}. (c) Here $T_{max} = T_{max}(\Delta M_{TR}/M_{TR})$. Scaling parameter β as a function of T/T_{SG} or T/T_{max}. Blue and purple dashed vertical lines indicate T_N/T_{max} for $x = 0.04$ and 0.05, respectively. Data points for $x = 0$ and 2.0 are taken from previous studies [3,5].

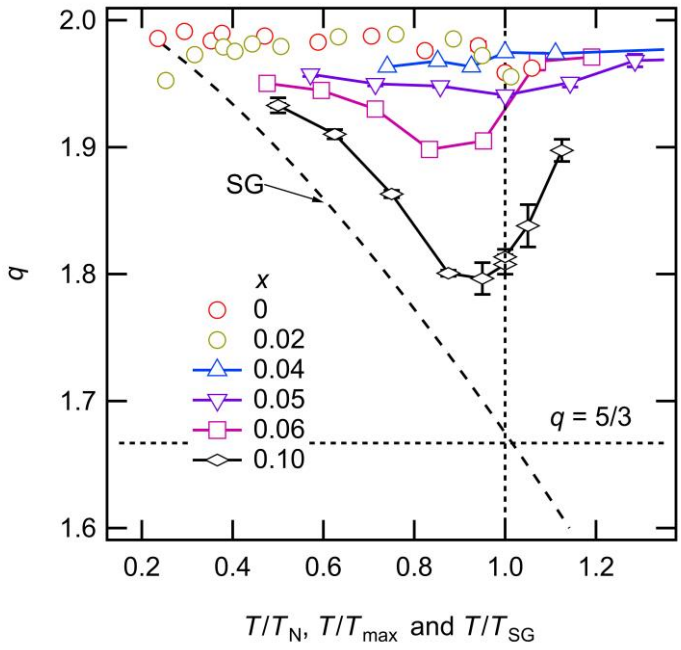

FIG. 14. Non-extensive parameter q as a function of reduced temperature T/T_N, T/T_{max}, and T/T_{SG} for $0 \leq x \leq 0.02$, $0.04 \leq x \leq 0.05$, and $0.06 \leq x$, respectively. Here $T_{max} = T_{max}(\Delta M_{TR}/M_{TR})$. Data points for $x = 0$ and 2.0 are taken from a previous study [5]. Dashed curve represents experimental results for spin glasses [5,19] (see text).

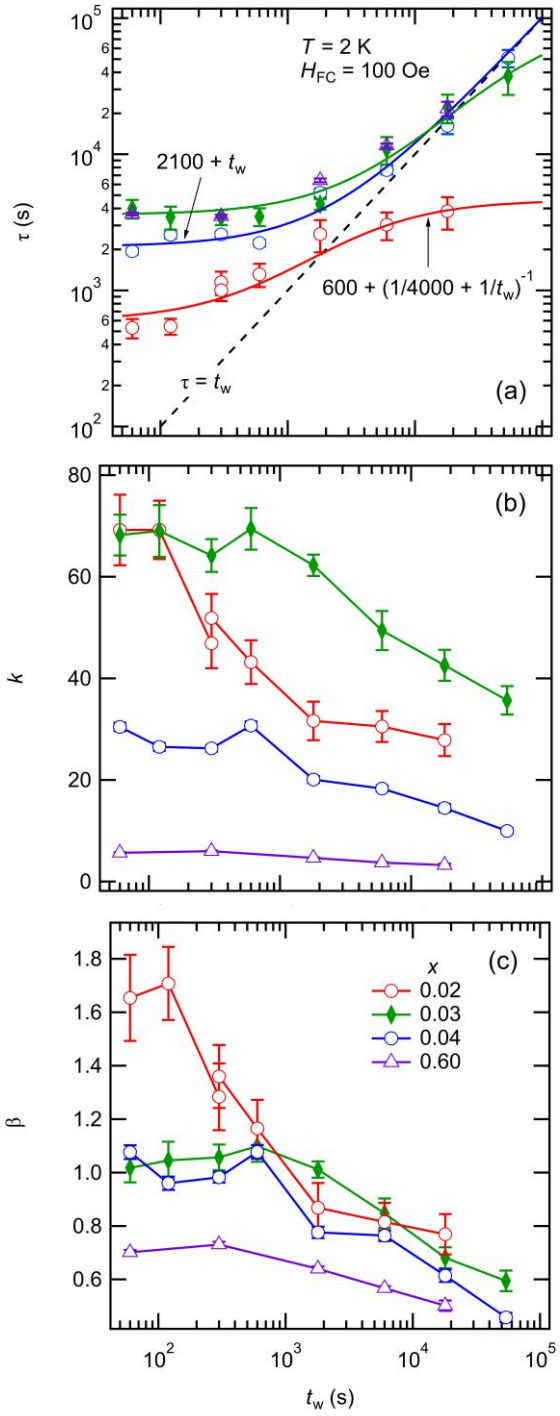

FIG. 15. Relaxation parameters (a) τ, (b) k, and (c) β extracted from the curve of thermoremanent magnetization intensity, $M_{TR}(t_w, t)$, as a function of t_w in the vicinity of x = 0.03 (η = 0.064) and at x = 0.60 (η = 0.342).

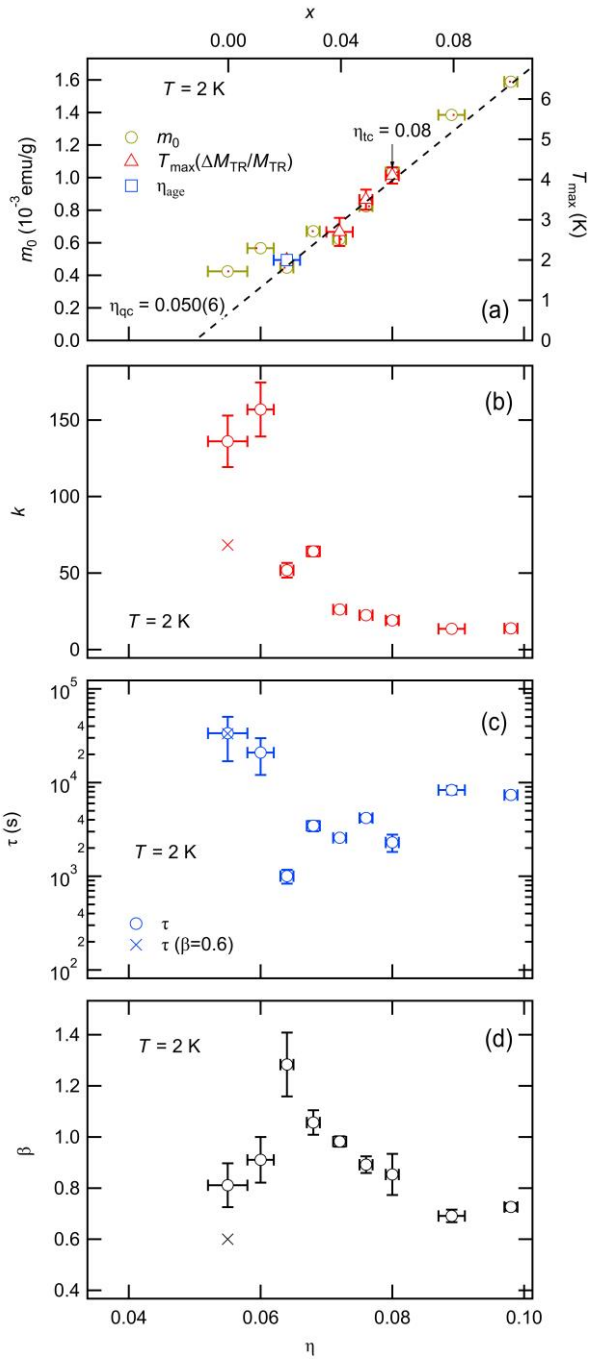

FIG. 16. Variations of (a) $m_0 = M_{TR}(T = 2\text{K}, t = 0)$ and $T_{max}(\Delta M_{TR}/M_{TR})$, (b) k, (c) τ, and (d) β with inversion η for $0 \le x \le 0.10$. The anomalous point $(\eta_{age}, T) = (0.066, 2\text{ K})$ observed in the t_w-dependence of τ in Fig. 15(a) is also plotted in (a). Black dashed line shows the linear variations of thermoremanent magnetization, M_{TR}, and $T_{max}(\Delta M_{TR}/M_{TR})$ with respect to η to give an estimation of the QCP η_{cq} at $T = 0$. In (b) – (d), ×'s represent the values for $x = 0$ with $\beta = 0.6$ [3]. Vertical arrow in (a) indicates the tricritical point η_{tc}.